



The Influence of Different Overburden Conditions to the Detectability of Controlled-Source Audio-Frequency Magnetotellurics at a Deep Depth

LI LIN^{1,2}, GUO JINGXUE², CUI XIANGBIN², WU YANGANG¹ AND YANG YUE¹

¹College of GeoExploration Science and Technology, Jilin University, Changchun 130026, China

²Polar Research Institute of China, Shanghai 200120, China

Email: lilin14@mails.jlu.edu.cn

Abstract: Based on the theory of three-dimensional forward and inverse modeling of controlled source audio frequency magnetotellurics (CSAMT), we devised a working apparatus model according to current real working conditions in the field. This model carried out several 3D forward and inverse calculations using different values of the thickness-to-depth ratio of anomaly, the difference between anomaly resistivity and wall rock resistivity, and conductive characteristics of low-resistive overburden. The influence of different overburden conditions to the detectability of CSAMT at a deep depth is analyzed and summarized. The calculation results show that: (1) Under the existence of low-resistive overburden, by using similar model parameters, an anomaly is resolvable at the burial depth of about 500m. An anomaly buried 700m deep can be poorly resolved. (2) After the overburden layer is removed, the inversion effect improves significantly for anomalies of the same size. At a shallow depth, the anomaly's inverted value approaches the actual one in relation to size, location and resistivity. The depth displayed by inverse modeling of an anomaly buried relatively deeply is generally lower than it actually is. (3) In uniform half-space, a general conclusion is that a low-resistive anomaly will be resolved if its thickness-to-depth ratio exceeds 0.22 times the square root of the ratio of anomaly resistivity to background resistivity. The inversion effect is no longer good to resolve an anomaly buried over 1600m beneath the surface.

Keywords: CSAMT, three-dimensional, overburden, investigation at a deep depth, resolvability

1. Introduction

To overcome the much difficulty of investigation caused by weak signals and arbitrary magnetotelluric sources, D.W.Strangway, known as a Canadian professor, proposed the method of CSAMT in 1971. Due to its high working efficiency, the wide range of investigation depth, superior resolvability and low susceptibility to shielding effect from overburden, the technique has found prompt application to various fields including oil exploration, gas exploration, geothermy, hydrology and metallic minerals. In particular, CSAMT develops rapidly with respect to hidden deposit detection and geologic structure identification. In recent years, China witnesses an increasing demand for mineral products and emphasis on ore and mineral searching in mine areas developed before. Against this backdrop, 3D ore investigation at deep depths becomes an engineering focus, raising a claim for stronger and stronger resolvability of any particular exploration method employed to detect deeply situated structures.

In summary, the massive factors influencing the effective investigation depth of CSAMT can be categorized into subjective and objective. Subjective elements contain working apparatus (such as transmitter, receiver, their distance, observation parameter component, and working frequency) [1-5], non-far field data [6], cultural noise, etc. Objective elements are composed of geoelectric structure characteristics and anomaly parameters like

conductivity difference, shape, occurrence, and its relative size against depth. Thick buried layers, such as basement, are better resolved than intermediate layers. 2D and 3D bodies are often harder to resolve than layers at an equivalent depth [7]. He Jishan [8] indicated that the investigation depth of CSAMT is or so, and that the horizontal resolvability at deep depths is a function of signal wavelength and its arrangement and size. At bands of low frequency, long wave signals present worse resolvability due to the expansion of investigation domain. Therefore, theoretically speaking, investigation depth can reach up to 2km with currently-used frequency range and transmitting power allowed. Most of research viewpoints on resolvability at deep depths are based on one-dimensional and two-dimensional controlled-source forward and inverse modeling as well as in-situ investigation situations in the field [9-11].

In the field work, the impact of the overburden cannot be ignored. It will reduce the accuracy of measurement results and the mine well rate. The resistivity of the overburden is generally smaller than that of the surrounding rock, and the larger the thickness is, the more serious the low resistance phenomenon is [12]. It is very important to study the influence of overburden on the CSAMT method to eliminate the interference and improve the exploration accuracy. The above mentioned factors influencing resolvability of CSAMT are more likely coupled than independently working. To highlight the essence of CSAMT, we simplified our discussion towards the

mere objective factors. Based on the theory of three-dimensional forward and inverse modeling and three-dimensional limited-memory quasi-Newton inversion, we devised a working apparatus model according to current real working conditions in the field. This model carried out several three-dimensional forward and inverse calculations with different values of the thickness-to-depth ratio of anomaly, the difference between anomaly resistivity and wall rock resistivity, and conductive characteristics of low-resistive layer. The influence of different overburden conditions to the detectability of CSAMT at a deep depth is analyzed and summarized.

2. Fundamental Theory

2.1 The Theory of Forward Modeling

We compute the 3D controlled-source electromagnetic field generated by finite-length wire sources in frequency domain by using Helmholtz equation:

$$\nabla \times \nabla \times \mathbf{e}_s - k^2 \mathbf{e}_s = (k^2 - k_p^2) \mathbf{e}_p \quad (1)$$

Where k_p denotes the complex wave number of medium in background field, k is the complex wave number of anomaly-included medium, \mathbf{e}_p is the Green's function of the background field, \mathbf{e}_s represents the induction field generated from anomalies [13]. Since the secondary field is solely linked to the primary field, Equation (1) is directly usable to find solutions to the anomalous secondary field of the central point on the boundary of subdivision elements. We compute the background field by means of de-singularized imaginary boundary surface [14-16], and the value of Hankel integral by means of numerical integration method [17-18]. Mathematical simulation is undertaken on the induction field by using staggered-grid finite difference technique [19]. The corresponding total electric field is expressed as

$$\mathbf{e} = \mathbf{e}_s + \mathbf{e}_p \quad (2)$$

The 3D distribution of the magnetic field at the center of some panels is calculated by applying the total electric field computed before to the equation

$$\mathbf{b} = -\frac{\nabla \times \mathbf{e}}{i\omega} \quad (3)$$

2.2 The Theory of Limited-Memory Quasi-Newton Inversion

To obtain suitable data inversion explanations, the on-surface controlled-source electromagnetic investigation data yet to be inverted is used as the impedance Z_{xy} , and is recorded as data vector \mathbf{d} . $F(\mathbf{m})$ is defined as the forward operator that maps model

vector \mathbf{m} into data vector $\hat{\mathbf{d}}$. Thus, by calculating the minimum value of targeted function (4), the 3D electromagnetic data inversion is aimed at acquiring a model parameter \mathbf{m} which allows the anticipated data $\hat{\mathbf{d}}$ to simultaneously satisfy a particular limitation and have the best fit to the survey data \mathbf{d} .

$$U(\lambda, \mathbf{m}) = (\mathbf{m} - \mathbf{m}_0)^T \mathbf{C}_m^{-1} (\mathbf{m} - \mathbf{m}_0) + \lambda^{-1} \left\{ (\mathbf{d} - \mathbf{F}[\mathbf{m}])^T \mathbf{C}_d^{-1} (\mathbf{d} - \mathbf{F}[\mathbf{m}]) - \chi_*^2 \right\} \quad (4)$$

In the above equation, \mathbf{C}_d is the data variance matrix, \mathbf{C}_m is the model variance function which sets limitations on the amplitude and smoothness of the model variance \mathbf{m}_0 (referring to the former model). The regularization parameter λ balances the weight of data derivation and model constraint during solution-seeking [20]. To optimize equation (4), the gradient operator computational principle of nonlinear conjugate gradient method [21-24] is used in the paper to transplant it to the limited-memory BFGS quasi-Newton inversion [25], so that realizing L-BFGS-based controlled-source electromagnetic investigation data inversion.

During iteration of quasi-Newton inversion, on the basis of BFGS calibration formula, we conduct approximate calculation on the second derivative (Hessian matrix) of the targeted function by using the latest \mathbf{m} iteration results. This measure reduces memory, and improves the precision and efficiency of computation. The value of \mathbf{m} can be found according to several factors including targeted function vector, calculation time required for inversion, and computer memory. In general conditions, the demand for precision can be met when $\mathbf{m}=3\sim 20$. To achieve relatively high inversion precision, we let \mathbf{m} be uniformly 820.

3. Computation Result

3.1 Model Parameter

A 1500-meter-long wire source is built in the transmitter. The six transmitting frequencies are 0.125 Hz, 16 Hz, 128 Hz, 512 Hz, 2048 Hz, 8192Hz. Figure 1 is details of apparatus parameter.

Given the tremendous computation load of CSAMT 3D forward and inverse modeling, we design a pair of typical theoretical models to discuss the aforementioned evaluation indices of currently-used controlled-source working apparatuses in the field. Model 1 is a single low-resistive anomaly buried in a homogeneous half-space. Corresponding parameters are: wall rock resistivity 500 $\Omega\cdot\text{m}$, changes of anomaly resistivity 5 $\Omega\cdot\text{m}$, 50 $\Omega\cdot\text{m}$, 100 $\Omega\cdot\text{m}$, 300 $\Omega\cdot\text{m}$; Model 2 is a single anomaly in the low-resistive overburden condition, whose parameters are: overburden thickness 100m, changes of anomaly resistivity 50 $\Omega\cdot\text{m}$, 100 $\Omega\cdot\text{m}$, 200 $\Omega\cdot\text{m}$, 300 $\Omega\cdot\text{m}$, wall

rock resistivity 500 Ω·m, anomaly resistivity fixed at 5 Ω·m.

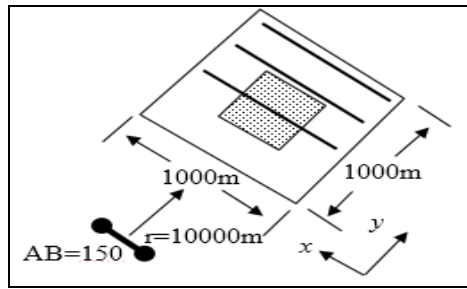


Fig. 1: parameters of the controlled source device model

The size of the 3D anomaly model is 200m×200m×200m, equivalent to a sphere with a radius of 124m.

Table 1 is the radius-to-depth ratio of anomaly in model 1.

Table 1: the radius-to-depth ratio of anomaly in model 1

d(m)	0	400	800	1200
R/d	Inf	0.31	0.155	0.077

We use the DC resistivity method proposed by He Jishan et al. as an example. Research findings show that at the conductivity difference of 1/100, a local anomaly will be difficult to resolve if the radius-to-depth ratio exceeds 1/10. Accordingly, we refer to Table 1 and determine the deepest depth of anomaly should be 1200m in this research. In terms of model 2, due to the existence of the overburden, the depth of anomaly is 100m, 300m, 500m and 900m, respectively.

There are 21 profiles and 441 measure points in the area of investigation. As a matter of convenience, our research objectives are two typical measure points (a point d0 is on the boundary of the survey area, and the other point d220 is at the center of the anomaly) and a survey line passing through the parallel source of the anomaly. Their locations are shown in Figure 2, from which d0 is 770m far from the anomaly center horizontally.

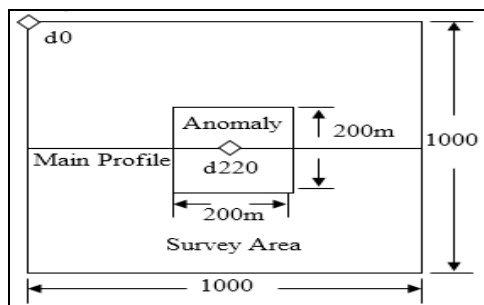


Fig. 2: The distribution of survey area and the position of typical points and profile

The grid size of some initial models is 50m×50m. The first layer of ground surface is as thick as 100m, and the rest thicken at the ratio of 1.1. We add Gaussian noise (maximum absolute value of 5%) to the forward modeling result to prepare survey data. The effective number of grids is 20×20×25. With extended grids counted in, the actual number of grids for inversion is 27,000. The inversion starts in the homogeneous half space. The host computer configuration is HP R910 server, RAM 128G, 4CPU,40 core, main frequency 2.56GHz. Each iteration of one model costs 3-4 minutes, and each model is iterated at 829 times at most [26]. Thus, the total time required for the computation load of the 33 models is about 1,600 hours.

3.2 Analysis of local low-resistive anomalies in a homogenous half space

We use the relative anomaly change to assess anomaly resolvability. Below are the formulas of relative error of anomaly:

$$\eta_{Re} = \frac{|\text{Re}[Z_{xy}]| - |\text{Re}[Z_{xy}^0]|}{|\text{Re}[Z_{xy}^0]|} \times 100\% \tag{5}$$

$$\eta_{Im} = \frac{|\text{Im}[Z_{xy}]| - |\text{Im}[Z_{xy}^0]|}{|\text{Im}[Z_{xy}^0]|} \times 100\% \tag{6}$$

Where Z_{xy} includes the resistance response of anomaly, and Z_{xy}^0 excludes that.

For anomalies of different ratios of anomaly resistivity to wall rock resistivity, we change anomaly depth to compute the relative change of frequency response of typical measure points and resistance data on the main profile.

Due to limited space, our case study is merely done at the anomaly resistivity of 5 Ω·m and the transmitting frequency of 128Hz. Figure 3 is the characteristics of profile frequency response.

As can be seen from Figure 3, when the anomaly resistivity is 5 Ω·m, the relative change of survey data plummets as the burial depth increases; for areas above the anomaly, the relative change of survey data decreases from 96% when the anomaly is placed on the ground to 0.2% when the burial depth is 1200m. According to the standard that the 2% error change is the investigation sensitivity of field data, we conclude that an anomaly is distinguishable at the resistivity of 5Ω·m and the burial depth of 600m, which is equal to a radius-to-depth ratio of 0.23, and that an anomaly is hard to resolve at deeper depth or with smaller radius-to-depth ratio.

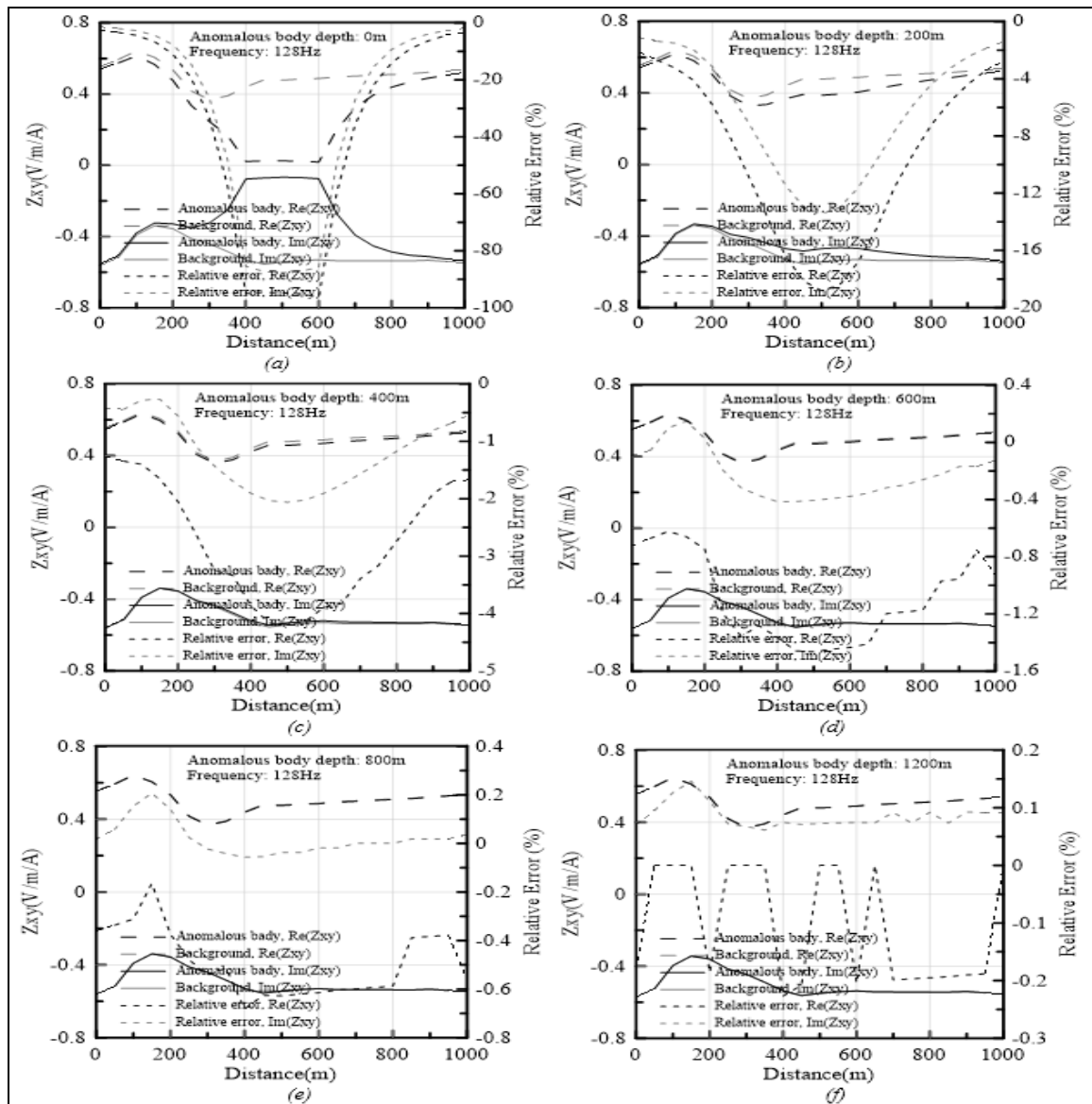


Fig. 3: The frequency response curve of main profile at different burial depths

Through the analysis of response resolvability of anomalies with 4 different values of resistivity at various burial depths, we summarized their basic features as follows:

- 1) 5Ω-m anomaly, at the burial depth of about 600m, equal to the radius-to-depth ratio $r/d=0.23$, distinguishable.
- 2) 50Ω-m anomaly, at the burial depth of about 500m, equal to the radius-to-depth ratio $r/d=0.25$, distinguishable.
- 3) 100Ω-m anomaly, at the burial depth of about 400m, equal to the radius-to-depth ratio $r/d=0.3$, distinguishable.
- 4) 300Ω-m anomaly, at the burial depth of about 200m, equal to the radius-to-depth ratio $r/d=0.6$, distinguishable.

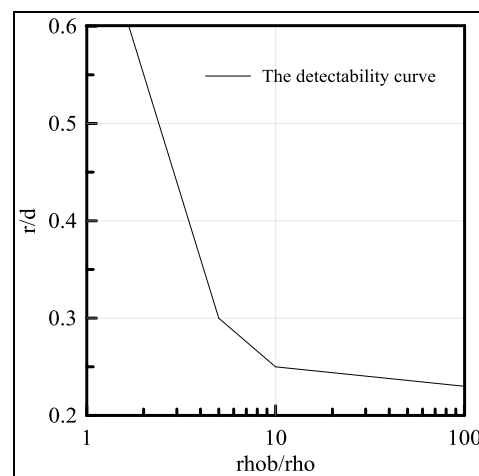
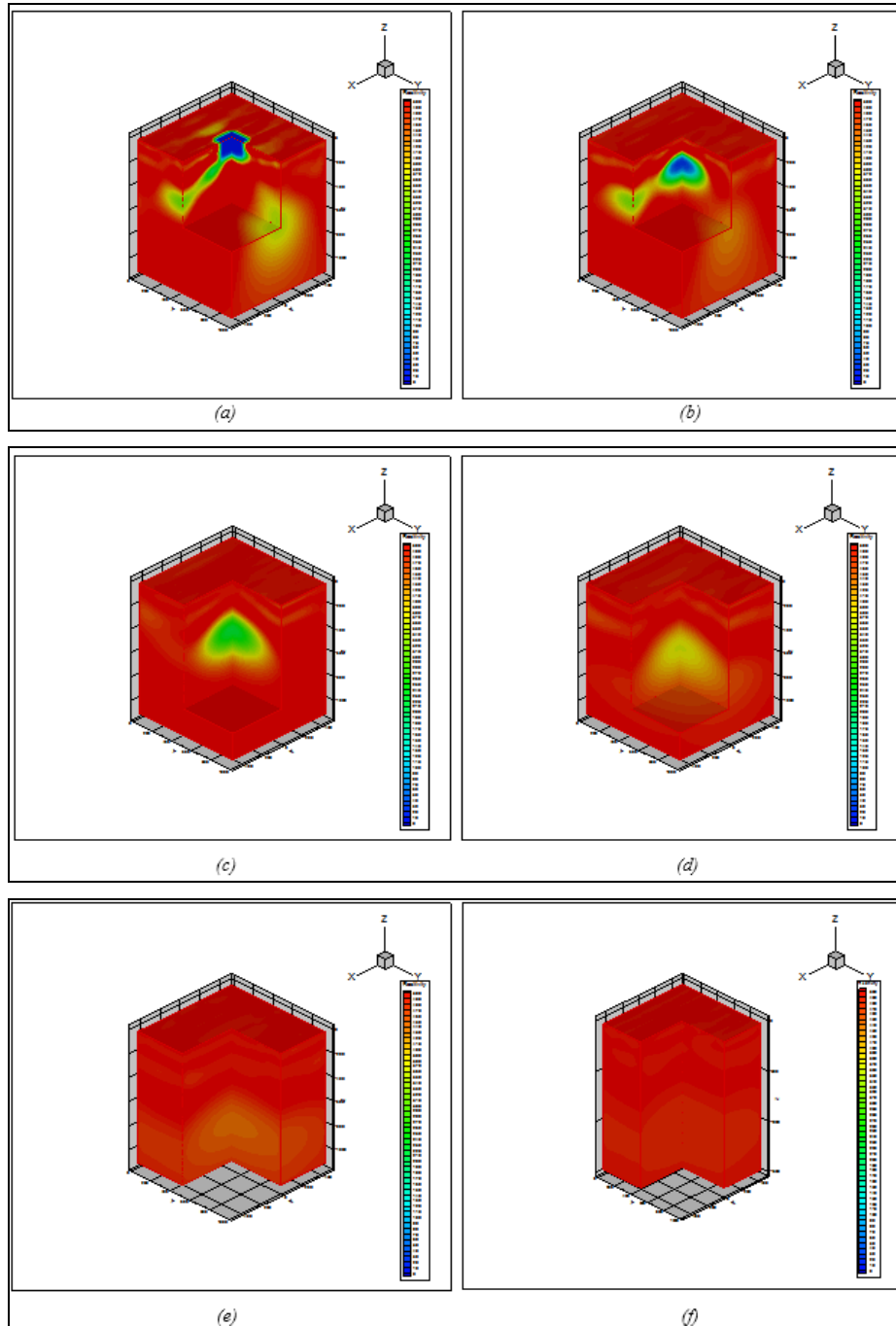


Fig. 4: The detectability curve

Figure 4 is the detectability of the equivalent sphere in a homogeneous half space. The x-coordinate denotes the ratio of wall rock resistivity to anomaly

resistivity(ρ_{ob}/ρ_0), and y -coordinate is the radius-to-depth ratio of the anomaly (r/d). As can be seen from this figure, detection depth drops greatly as ρ_{ob}/ρ_0 lowers down.

The 3D inversion is also conducted at the anomaly resistivity of $5 \Omega\cdot m$, with maximum 820 iterations. The fitted curve converges constantly and basically becomes stable and downward after 820 iterations. It can be anticipated that the inversion result will further approach the actual value if iteration continues on.



(a). anomaly at the burial depth of about 0m; (b). anomaly at the burial depth of about 200m; (c). anomaly at the burial depth of about 400m; (d). anomaly at the burial depth of about 600m; (e). anomaly at the burial depth of about 800m; (f). anomaly at the burial depth of about 1200m.

Fig. 5 The 3D inversion results

Inversion is necessary to determine anomaly detectability. In terms of a 3D anomaly model, the difference between 3D inversion result and theoretical result needs to be measured according to both

conductivity change and the spatial form of anomaly distribution. As the 3D inversion model is smooth, resistivity in the distribution area of anomaly changes gradually. Therefore, the method of model error

evaluation that fits for one-dimensional models may be inapplicable herein.

Conceptually, in the inversion result of resistivity distribution, if there exists resistivity anomaly and its center and the theoretical center coincide, and if their trends of resistivity changes are identical, the 3D anomaly can be resolved.

On this premise, we divide the level of resolvability of the minimum targeted structure into three sublevels: readily resolvable, resolvable, and unresolvable. For lack of related research reference, we attempt to define the specific requirements for the triple of sublevels as follows:

Readily resolvable: 1)the anomaly resistivity approaches the ideal value (possible quantitative conditions of error:①<20%;②>20%;③no response);2)the anomaly form is complete and approaches the ideal form; 3)the anomaly position is relatively accurate (possible quantitative conditions of h, 2b, 2d errors:①<20%;②>20%;③no response)

Resolvable: satisfies any two of the three conditions above.

Unresolvable: the inversion result has neither form response nor resistivity response.

As shown in Figure 5, for an anomaly at shallow depth, its position, size and resistivity approach the actual values by using inverse modelling. An anomaly can be clearly located at the burial depth of 800m, which validates the correctness of limited-memory quasi-Newton inversion method. For 4 anomalies of different values of resistivity, we evaluate their resolvability with three indices: depth, resistivity, and the product of width and thickness. According to resolvability analysis, the basic features of depth inversion are:

- 1) 5Ω·m anomaly, at the burial depth of about 1200m, equal to the radius-to-depth ratio $r/d=0.1$, distinguishable.
- 2) 50Ω·m anomaly, at the burial depth of about 1200m, equal to the radius-to-depth ratio $r/d=0.1$, distinguishable.
- 3) 100Ω·m anomaly, at the burial depth of about 1100m, equal to the radius-to-depth ratio $r/d=0.11$, distinguishable.
- 4) 300Ω·m anomaly, at the burial depth of about 1100m, equal to the radius-to-depth ratio $r/d=0.11$, distinguishable.

The basic features of resistivity inversion are:

- 1) 5Ω·m anomaly, at the burial depth of about 200m, equal to the radius-to-depth ratio $r/d=0.62$, distinguishable.
- 2) 50Ω·m anomaly, at the burial depth of about 200m, equal to the radius-to-depth ratio $r/d=0.62$, distinguishable.
- 3) 100Ω·m anomaly, at the burial depth of about

100m, equal to the radius-to-depth ratio $r/d=1.24$, distinguishable.

- 4) 300Ω·m anomaly, at the burial depth of about 100m, equal to the radius-to-depth ratio $r/d=1.24$, distinguishable.

The basic features of scale inversion are:

- 1) 5Ω·m anomaly, at the burial depth of about 600m, equal to the radius-to-depth ratio $r/d=0.2$, distinguishable.
- 2) 50Ω·m anomaly, at the burial depth of about 600m, equal to the radius-to-depth ratio $r/d=0.248$, distinguishable..
- 3) 3)100Ω·m anomaly, at the burial depth of about 500m, equal to the radius-to-depth ratio $r/d=0.248$, distinguishable.
- 4) 4)300Ω·m anomaly, at the burial depth of about 400m, equal to the radius-to-depth ratio $r/d=0.31$, distinguishable.

We plot the obtained basic characteristics in Figure 6, in which the x-coordinate denotes the ratio of wall rock resistivity to anomaly resistivity(ρ_{ob}/ρ_a),and y-coordinate is the radius-to-depth ratio of the anomaly(r/d).

As a whole, the trend of depth-varying curves for anomalies of different values of resistivity are basically the same. The shallower the anomaly is buried, the higher the resolvability is, and the more similar the anomaly resistivity, size and depth is to the actual values. According to Figure 6, the decrease in ρ_{ob}/ρ_a causes the resolvability to drop. What is more, if the anomaly is buried deeply, the inversed depth is generally smaller than the actual one.

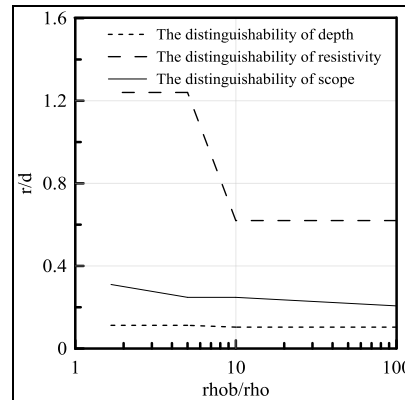


Fig. 6: The distinguishability curve

In terms of low-resistive anomalies, by comparing inversion results, we deem that there is a likely critical point for the designed anomaly(size 200m×200m×200m, burial depth 1200m, anomaly resistivity 300Ω·m, wall rock resistivity 500Ω·m): An anomaly with the planar size of 200m*200m will be resolved if its thickness-to-depth ratio exceeds 0.22 times the square root of the ratio of anomaly resistivity to background resistivity. The inversion

effect is no longer good to resolve an anomaly buried over 1600m beneath the surface.

In terms of low-resistive anomalies, by comparing inversion results, we deem that there is a likely critical point for the designed anomaly(size 200m×200m×200m, burial depth 1200m, anomaly resistivity 300Ω·m, wall rock resistivity 500Ω·m): An anomaly with the planar size of 200m*200m will be

resolved if its thickness-to-depth ratio exceeds 0.22 times the square root of the ratio of anomaly resistivity to background resistivity. The inversion effect is no longer good to resolve an anomaly buried over 1600m beneath the surface.

3.3 analysis of local low-resistive anomaly under the existence of overburden

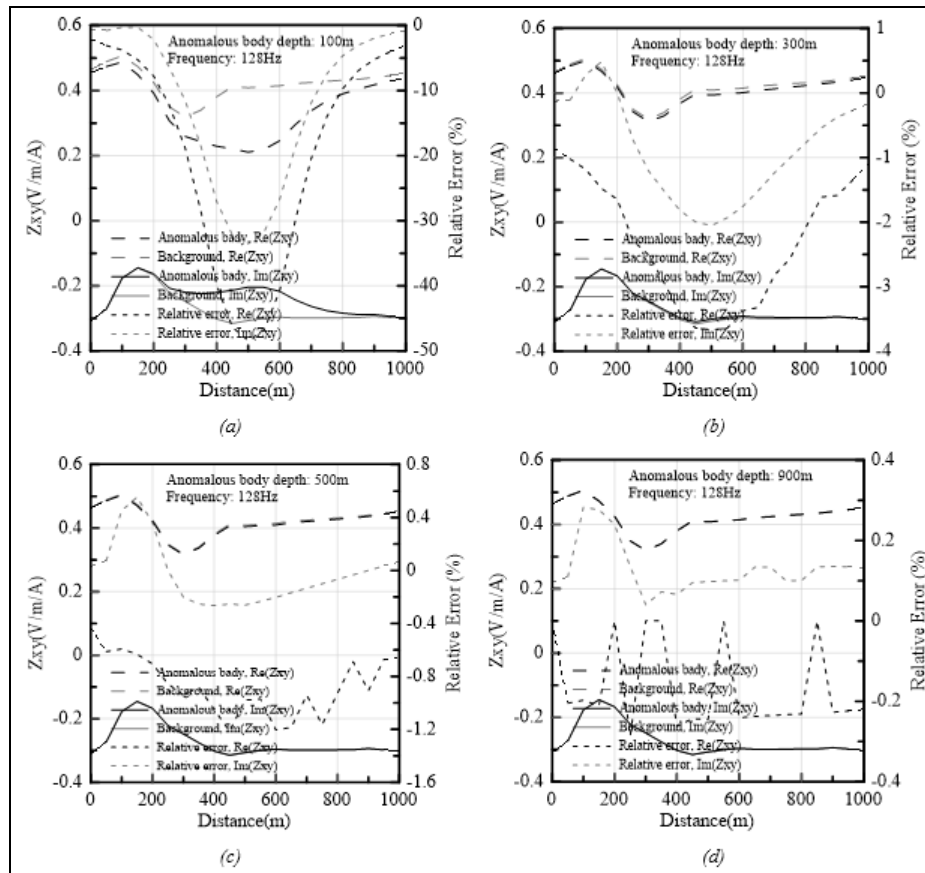


Fig. 7: The frequency response curve of main profile under the existence of overburden

Through the analysis of the response detectability of an anomaly under the existence of 4 overburdens with different values of resistivity, we summarize the resolvability of the equivalent sphere at a homogeneous half space, as shown in Figure 8. The x-coordinate denote the ratio of wall rock resistivity to anomaly resistivity(ρ_{ob}/ρ_a), and y-coordinate is the radius-to-depth ratio of the anomaly(r/d). According to Figure 8, the trend of relationship between investigation depth and ρ_{ob}/ρ_a is obviously, i.e. the investigation depth increases prominently as ρ_{ob}/ρ_a decreases.

3D inversion is also conducted at the overburden resistivity of 100Ω·m. The iteration is done at 820 times at most. For 4 low-resistive overburdens of different values of resistivity, we evaluate resolvability from the perspectives of depth, resistivity, and the product of width and depth. The correspondingly obtained basic features are plotted in Figure 10. The x-coordinate denotes the ratio of wall

rock resistivity to anomaly resistivity(ρ_{ob}/ρ_a), and y-coordinate is the radius-to-depth ratio of the anomaly(r/d).

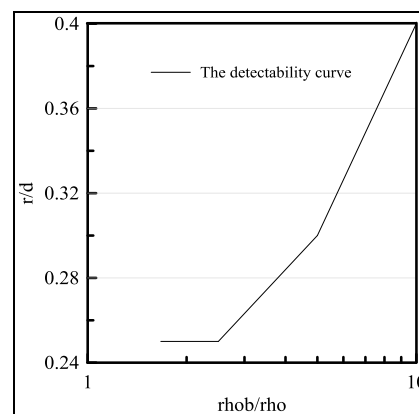


Fig. 8: The detectability curve under the existence of overburden

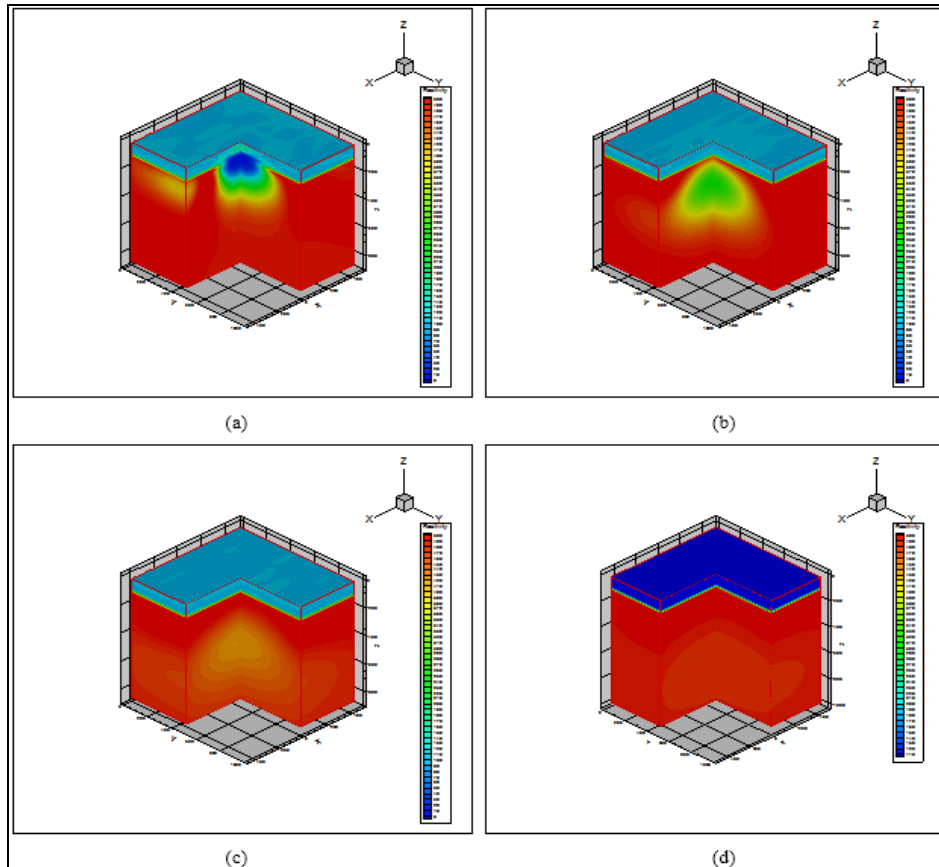


Fig. 9: The 3D inversion results under the existence of overburden

According to Figure 10, as ρ_{ob}/ρ_a decreases, the resolvability improves as a result. Also, the trends reflected by different resolvable indices are basically the same. The forward-inverse relative error result and the 3D inversion result show that under the existence of low-resistive overburden of different values of resistivity, an anomaly at a shallow depth is more sensitive to high frequency during investigation, while the low-frequency inversion effect is better and better as the burial depth increases. The mere use of 0.125Hz is enough to distinguish an anomaly at the burial depth of 500m or more.

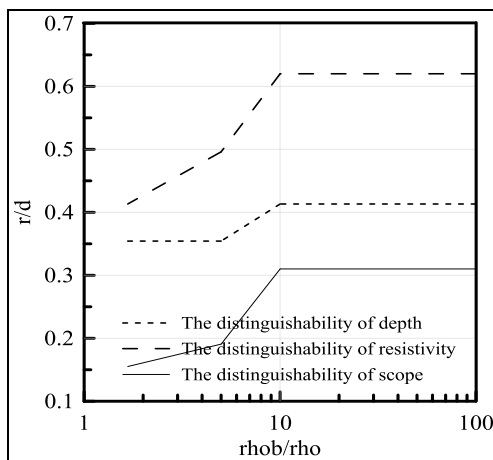


Fig. 10: The distinguishability curve under the existence of overburden

The resolvability becomes stronger as overburden resistivity approaches wall rock resistivity, especially when the anomaly is buried shallowly. If the burial depth increases up to 500m, such resistivity difference has barely no effect on resolvability. Deeper depth corresponds to a plunge in resolvability. The relative error rate has been below 1% when the anomaly is buried 900mm beneath the surface, and an anomaly of less than 200Ω·m cannot be resolved according to the inversion result.

4. Conclusion

Based on the theory of three-dimensional forward and inverse modeling of CSAMT, we devised a working apparatus model according to current real working conditions in the field. This model carried out several three-dimensional forward and inverse calculations. The influence of different overburden conditions to the detectability of CSAMT at a deep depth is analyzed and summarized. The calculation results of overall model tests show that:

- (1) With or without overburden, the trend of depth-varying curves of anomalies of different resistivity is basically the same. The shallower the anomaly is buried, the higher the resolvability is, and the more similar the anomaly resistivity, size and depth is to the actual values. The depth displayed by inverse modeling of an anomaly buried relatively deeply is generally lower than it

actually is.

- (2) For an anomaly buried shallowly (more sensitive to high frequency), the relative error of imaginary part and the relative error of real part are little, albeit bigger for the former one. For an anomaly buried deeply, the relative error of real part at low-frequency points is big.
- (3) In uniform half-space, an anomaly at a shallow depth is more sensitive to high frequency during investigation, while the low-frequency inversion effect is better and better as the burial depth increases. If situated up to the depth in the range of 400m-800m contrast with respect to shallower depths, an anomaly will be better located by using the 128Hz-512Hz relative error curve. This phenomenon is more obvious as a response to the rise in anomaly resistivity. During the model test, an anomaly buried deeply only respond to the frequency of 0.125Hz.
- (4) Under the existence of low-resistive overburden, by using similar model parameters, an anomaly is resolvable at the burial depth of about 500m. An anomaly buried 700m deep can be poorly resolved. After the overburden is removed, the inversion effect improves significantly for anomalies of the same size. At a shallow depth, the anomaly's inversed value approaches the actual one in relation to size, location and resistivity. The maximum burial depth that guarantees resolvability is 1,200m or so.
- (5) Overall, in uniform half-space, a low-resistive anomaly of similar size as the sample anomaly will be resolved if its thickness-to-depth ratio exceeds 0.22 times the square root of the ratio of anomaly resistivity to background resistivity. The inversion effect is no longer good to resolve an anomaly buried over 1600m beneath the surface.
- (6) The fitted curve converges constantly and basically becomes stable and downward after 820 iterations. The model is hardly iterated so many for an anomaly that is buried deeply and blocked by low-resistive overburden. It can be anticipated that the inversion result will further approach the actual value if iteration continues on.

5. Acknowledgements

Thanks to Prof. Weng Aihua for the help to this paper.

References

- [1] Y. Wang, Research on Joint Time-Frequency Electromagnetic Method in Deep Mine Resources Prospecting, Chang Chun, Jilin University, 2011.
- [2] A.H. Weng, D.J. Li, Y.B. Li, "Selection of Observing Parameters in Controlled Source Electromagnetic Method", *Chinese Journal of Geophysics*, 02., P697-P708., 2015.
- [3] R. Streich, M. Becken, "Electromagnetic Fields Generated by Finite-Length Wire Sources: Comparison with Point Dipole Solutions", *Geophysical Prospecting*, 59. 2., P361-P374., 2011.
- [4] S.R. Li, A.H. Weng and D.J. Li, "Influence of Wire Length on Deep Three-Dimensional Controlled Source Electromagnetic Method", *Progress in Geophysics*, 30. 4., P1734-P1742., 2015.
- [5] Y. Yang, Y.B. Li and A.H. Weng, "Effect of The Choice of Frequency on Three-Dimensional Controlled Source Electromagnetic Inversion", *Progress in Geophysics*, 30. 2., P829-P835., 2015.
- [6] N.B. Boschetto, G.W. Hohmann, "Controlled-Source Audiofrequency Magnetotelluric Responses of Three-Dimensional Bodies", *Geophysics*, 56. 2., P255-P264., 1991.
- [7] S.E. Rafiee, M.M. Sadeghiazad, "3D numerical analysis on the effect of rounding off edge radius on thermal separation inside a vortex tube", *International Journal of Heat and Technology*, 31. 1., P83-P90., 2015.
- [8] J.S. He, *Controlled Source Audio-Frequency Magneto-Telluric Method*, Chang Sha, Central South University Press, 1985.
- [9] H. Elvebakk, O.B. Lile, "Electromagnetic Depth Sounding with CSAMT in Norway", *Geoexploration*, 24. 3., P271-P272., 1987.
- [10] T. Koichi, "Imaging Geothermal Fractures by CSAMT Method at Takigami Area in Japan", *Memoirs of the Faculty of Engineering*, 63. 1., P23-P37., 2003.
- [11] Y.S. Zhong, Z.Q. Han, J. Luo, "A Tentative Discussion on the Detecting Depth of Controlled Source Audio Magneto Telluric Method", *Geophysical and Geochemical Exploration*, 39. 4., P768-P774., 2015.
- [12] C.F. Liu, H.F. Huang, X.P. Ma, "Problems of the electrical prospecting method of field water exploration and their solutions", *Advances in Science and Technology of Water Resources*, 28. 5., P74-P77., 2008.
- [13] M. Commer, G.A. Newman, "New Advances in Three-Dimensional Controlled-Source Electromagnetic Inversion", *Geophysical Journal International*, 172., P513-P535., 2008.
- [14] M. Goldman, *Non-conventional Methods in Geoelectrical Prospecting*, New York, Ellis Horwood Ltd Publisher, 1990.
- [15] U.A. Das, "Reformalism for Computing Frequency and Time-Domain EM Responses of a Buried, Finite-loop", Extended Abstracts, SEG Annual Meeting-1995, Houston, P811-P814., 1995.
- [16] A.H. Weng, Y.H. Liu, D.Y. Jia, "Compute Green's Function from Discontinuity of Tangential Electrical Fields Inside Source Contained Boundary", *Journal of Jilin University (Earth Science Edition)*, 43. 2., P603-P609., 2013.
- [17] A.D. Chave, "Numerical Integration of Related Hankel Transforms by Quadrature and Continued

- Fraction Expansion”, *Geophysics*, 48. 12., P1671-P1686., 1983.
- [18] A.H. Weng, X.Q. Wang, “Utilizing Direct Integration to Enhance Calculation Accuracy of 1D Electromagnetic Response for Current Dipole Source”, *Northwestern Seismological Journal*, 25. 3., P193-P197., 2003.
- [19] J.S. Shen, “Modeling of 3D Electromagnetic Responses in Frequency Domain by Using Staggered-Grid Finite Difference Method”, *Chinese Journal of Geophysics*, 46. 2., P281-P288., 2003.
- [20] G.D. Egbert, A. Kelbert, “Computational Recipes for Electromagnetic Inverse Problems”, *Geophysical Journal International*, 189., P251-P267., 2012.
- [21] G.A. Newman, D.L. Alumbaugh, “Three-Dimensional Massively Parallel Electromagnetic Inversion- I, Theory”, *Geophysical Journal International*, 128., P345-P354., 1997.
- [22] G.A. Newman, D.L. Alumbaugh, “Three-Dimensional Magnetotelluric Inversion Using Non-linear Conjugate Gradients”, *Geophysical Journal International*, 140., P410-P424., 2000.
- [23] G.A. Newman, M. Commer, J.J. Carazzone, “Imaging CSEM Data in the Presence of Electrical Anisotropy”, *Geophysics*, 75. 2., P51-P61., 2010.
- [24] A.H. Weng, Y.H. Liu, D.Y. Jia, “Three-Dimensional Controlled Source Electromagnetic Inversion Using Non-linear Conjugate Gradients”, *Chinese Journal of Geophysics*, 55. 10., P3506-P3515., 2012.
- [25] D. Avdeev, A. Avdeeva, “3D Magnetotelluric Inversion Using a Limited-Memory Quasi-Newton Optimization”, *Geophysics*, 74. 3., P45-P57., 2009.
- [26] W. Ambrosini, “Eigenvalues and Eigenvectors in computational modelling of one-dimensional flow dynamics”, *International Journal of Heat and Technology*, 21. 1., P3-P12., 2003.